Glial lipid droplets and neurodegeneration in a Drosophila model of complex I deficiency

Marie-Jeanne Cabirol-Pol, Bilal Khalil, Thomas Rival, Catherine Faivre-Sarrailh, Marie Besson

Glial lipid droplets and neurodegeneration in a *Drosophila* model of complex I deficiency

Marie-Jeanne Cabirol-Pol[1], Bilal Khalil[1,2], Thomas Rival[3], Catherine Faivre-Sarrailh[1*], Marie Thérèse Besson[1*]

[1] Aix Marseille Université, CNRS, CRN2M-UMR7286, 13344 Marseille cedex 15, Marseille, France.
[2] Present address: Department of Neuroscience, Mayo Clinic Florida, Jacksonville, FL 32224, USA.
[3] Aix Marseille Université, CNRS, IBDM, Marseille, France.
[*] Corresponding authors: catherine.sarrailh@univ-amu.fr or marie-therese.besson@univ-amu.fr

Address correspondence to : Catherine Faivre-Sarrailh, CNRS UMR 7286-CRN2M, Aix Marseille Université, 51 bd Pierre Dramard, 13344 MARSEILLE Cedex 15, France. Phone: 33 (0)4 91 69 88 80.

Running title: Loss of NDUFS8/ND23 induces glial degeneration

Abstract 220 words, Introduction 675 words, Materials and Methods 1414 words, Results 2401 words, Discussion 1694 words, Acknowledgments 77 words, References 2345 words, Legends 1901 words

Total 10890 words

Figures 8

Key words: Leigh syndrome, *Drosophila* brain, mitochondria, *ND23* subunit, lipid droplets

Main points: In *Drosophila* models of Leigh syndrome, glial knockdown of ND23 induces accumulation of lipid droplets and intense vacuolization. In contrast, neuronal knockdown causes discrete neurodegeneration but behavioral alterations and early lethality

ABSTRACT

Mitochondrial defects associated with respiratory chain complex I deficiency lead to heterogeneous fatal syndromes. While the role of NDUFS8, an essential subunit of the core assembly of the complex I, is established in mitochondrial diseases, the mechanisms underlying neuropathology are poorly understood. We developed a *Drosophila* model of *NDUFS8* deficiency by knocking down the expression of its fly homologue in neurons or in glial cells. Downregulating *ND23* in neurons resulted in shortened lifespan, and decreased locomotion. Although total brain ATP levels were decreased, histological analysis did not reveal any signs of neurodegeneration except for photoreceptors of the retina. Interestingly, *ND23* deficiency-associated phenotypes were rescued by overexpressing the glucose transporter *hGluT3* demonstrating that boosting glucose metabolism in neurons was sufficient to bypass altered mitochondrial functions and to confer neuroprotection. We then analyzed the consequences of *ND23* knockdown in glial cells. In contrast to neuronal knockdown, loss of *ND23* in glia did not lead to significant behavioral defects nor to reduced lifespan, but induced brain degeneration, as visualized by numerous vacuoles found all over the nervous tissue. This phenotype was accompanied by the massive accumulation of lipid droplets at the cortex-neuropile boundaries, suggesting an alteration of lipid metabolism in glia. These results demonstrate that complex I deficiency triggers metabolic alterations both in neurons and glial cells which may contribute to the neuropathology.

INTRODUCTION

Mitochondria perform numerous vital functions in cells, including major production of ATP through oxidative phosphorylation via the respiratory chain complexes. Complex I is the first and largest enzyme of the mitochondrial respiratory chain and plays critical roles in electron transfer and proton gradient formation leading to ATP synthesis. Complex I deficiencies (CID) are the most frequently occurring in the respiratory chain system and account for a heterogeneous group of fatal disorders that can be due to mutations in either the nuclear or mitochondrial genome. Clinical presentations may vary with organ specific heterogeneity, ranging from fatal neonatal to adult-onset syndromes including Leigh syndrome, encephalomyopathy, leukoencephalopathy, MELAS (mitochondrial encephalomyopathy, lactic acidosis, and stroke-like episodes) and NARP (neuropathy, ataxia and retinitis pigmentosa) syndromes (Fassone and Rahman, 2012; Koopman *et al.*, 2012). The majority of the affected patients suffer from Leigh syndrome, a fatal, incurable, rapidly progressive neurodegenerative disorder with an incidence of at least 1 case out of 40,000 live births (Gerards *et al.*, 2016; Lee *et al.*, 2016). Leigh syndrome features brain necrotic lesions characterized by spongiosis, neuronal loss, and astrocytosis associated with muscular hypotonia, developmental delay, abnormal eye movements, seizures, and ataxia (Leigh, 1951; Rahman *et al.*, 1996). So far, the exact mechanism underlying the neurodegeneration in these diseases is still unclear.

In eukaryotes, complex I consists of 44 subunits encoded either by mitochondrial or nuclear DNA (Vinothkumar *et al.*, 2014) for a molecular mass of approximately 1000 kDa (Wirth *et al.*, 2016). The fourteen subunits that form the catalytic core are conserved from bacteria to humans. Mutations in six mtDNA-encoded (ND1 to 6) and thirteen nuclear-encoded (NDUFS1 to 8; NDUFV1; NDUFA1, 2, 9, 10, and 12) complex I subunits have been correlated with Leigh syndrome (Rodenburg, 2016). *Drosophila* ND23 is homologous to the mammalian complex I subunit NDUFS8, also known as TYKY subunit (Porcelli *et al.*, 2007). This subunit is highly conserved among species, with an 83% amino acid homology between *Drosophila* and humans, and is present in both prokaryotes and eukaryotes. It is also one of the 14 subunits that constitute the minimal complex I unit that is sufficient to support enzymatic activity indicating its functional importance. NDUFS8 contains two [4Fe–4S] clusters which are required for electron transfer (Procaccio *et al.*, 1997). A mutation affecting NDUFS8 was firstly described by Loeffen *et al.* (1998) and provided the first link between the reduced activity of complex I and Leigh syndrome.

We established *Drosophila* models for CID by specific down-regulation of the *ND23* subunit expression using RNA interference (RNAi) in glial cells or in neurons. As previously described, knockdown of *ND23* in neurons causes shortened lifespan (Besson *et al.*, 2015). In the present study, we showed that it induced behavioral alterations such as reduced locomotor performance and neuronal degeneration in eyes and mushroom bodies, without other histopathological features. To understand whether glial cells play a role in the neuropathology, we investigated the effect of *ND23* RNAi expression

in this cell type. We showed that while the survival and motor behavior of flies were not affected, we unexpectedly observed intense vacuolization using light and electron microscopy, indicating brain degeneration. We also observed numerous lipid droplets (LDs) accumulated mostly in cortex glia which surround neuronal cell bodies and in neuropile glia which enwrap neurites and synapses. We investigated the metabolic changes induced by CID by overexpressing the human glucose transporter hGluT3 and determined that it restores ATP levels, locomotion and survival in *Drosophila* expressing *ND23* RNAi in neurons. Our data suggest that stimulating glucose metabolism might prove useful by overpassing respiratory chain deficiencies in neurons. However, in glial cells, lipid homeostasis seems altered since abundant LDs were present at the cortex-neuropile border. *ND23* knockdown in glial cells seems to preferentially alter lipid homeostasis, and consistently neurodegeneration and LDs accumulation were not rescued by hGluT3 overexpression. We describe here a novel *Drosophila* model of CID, which recapitulates the main features of human encephalopathies such as Leigh Syndrome, including neurodegeneration, shortened lifespan and motor disability.

MATERIALS AND METHODS

Drosophila stocks

The different strains were obtained from the Bloomington *Drosophila* Stock Center (Bloomington, Indiana). The strain carrying the phosphofructokinase transgene (*UAS-PFK*; line #4) was kindly provided by C.S. Thummel (Tennessen *et al.*, 2011) and the *UAS-perilipin-2*::*EYFP* line by R.P. Kühnlein (Bi *et al.*, 2012). The *hGluT3* flies were generated in Besson *et al.* (2015). The *ND23* RNAi line (v110797, P{KK102085}VIE-260B) was purchased from VDRC (Vienna, Austria). Flies w^{1118} (BL5905) were used as wild-type controls. Flies were raised on standard cornmeal agar diet. All crosses were performed at 19°C for egg laying. Developmental stages of crosses using the driver *repo-GAL4* were conducted at 25°C. In order to attenuate developmental effects, for all crosses using the driver *elav-GAL4*, the larval and pupal stages were raised at 19°C, and only the adult life was conducted at 25°C.

Lifespan experiments

Adult female flies were collected within 24 h of emergence in vials at a density of about 20 flies per vial and all adult flies were aged at 25°C on standard food. The vials were changed 3 times per week and dead flies were scored every day. Survival curves were generated from 2-4 experiments performed in the same conditions and representative survival curves were shown.

Locomotion assay

Locomotor performance was tested by the negative geotaxis test on different batches of flies at 1, 4 or 12 days of adulthood as described previously (Besson *et al.*, 2015). Flies were allowed to climb for 30 s. The test was repeated 3 times for each batch of 8 flies at 1 min interval between consecutive assays. The percentages of flies that reached the top of the column and of flies that remained at the bottom were separately calculated. Each experiment was repeated 3 times with approximately 40-80 flies for each genotype.

Pseudopupil analysis

Pseudopupil analysis (Franceschini and Kirschfeld, 1971) was carried out to visualize photoreceptor cells in the ommatidia of the compound eye. Each adult female head was dipped in vaselin grease covering a microscope slide to allow photoreceptor observation. Eyes were observed with a Leica TCS SP2 microscope using a x60 objective, and photographed with a CoolSnap HQ Photometrics camera. The imaging was performed with Photoshop CS (Adobe). The number of visible rhabdomeres per ommatidium was scored for 20 ommatidia per eye, and 6 to 12 flies were examined per genotype. Comparisons between distributions of photoreceptor number per ommatidium in each line were performed.

Measurements of cellular ATP levels

A luminescent ATP detection assay kit (Abcam, ab113849) was used to measure ATP concentrations according to manufacturer's instructions. For each preparation, five female adult brains were rapidly dissected at 4°C in PBS buffer. Luciferase activity was quantified using a Mithras LB 940 luminometer (Berthold technologies) with automated injection of 50 µl of luciferase reagent. Solutions of known ATP concentrations generated a standard curve. Final ATP concentrations were measured from at least three separate brain preparations and means ± SEM were expressed as percentage relative to controls.

Immunohistochemistry and image analysis

Drosophila brains were dissected in a cold PBS solution, fixed for 30 min in 4% buffered paraformaldehyde, rinsed 3 times in PBS with 0.1% Triton-X (PBS-T) and blocked with 5% normal goat serum for 30 min. After blocking, they were incubated overnight at 4°C in one or more of the following primary antibodies: rat anti-Elav (1:500; 7E8A10, DSHB), mouse anti-Repo (1:250; 8D12, DSHB); rabbit anti-GFP (1:500; Molecular Probes; Thermo Fisher Scientific, France), or mouse anti-fasciclin II (FasII) (1:100; 1D4, DSHB). The following day, brains were rinsed in PBS-T, and incubated for 2 h at room temperature in secondary antibody AlexaFluor 488 donkey anti-rabbit IgG and AlexaFluor 568 goat anti-mouse IgG (1:600; Molecular Probes) and in Hoechst 33342 (Molecular Probes) for nuclear staining. Following secondary incubation, brains were washed in PBS and mounted in Mowiol. All confocal images were acquired with a Zeiss LSM 710 confocal microscope, and processed using Zeiss software ZEN 2010 and Photoshop CS (Adobe) to adjust size, resolution, contrast, or brightness of the final images.

The neutral lipids were detected by the lipophilic fluorescent dyes Nile Red (Sigma, St. Louis, MO) (Greenspan *et al.*, 1985; Listenberger and Brown, 2007) or Bodipy 493/503 (Thermo Fisher Scientific) (Bi *et al.,* 2012). For this purpose, brains were rapidly dissected in cold PBS, fixed in 4% buffered paraformaldehyde for 30 min, and rinsed with PBS to remove fixative. Then, they were incubated for 15 min, protected from light, on an orbital shaker, at 1:100 dilution in PBS with 0.5 mg/ml Nile Red dissolved in DMSO or for 30 min with Bodipy (1 µg/ml). Subsequently the brains were rinsed 3 times with PBS and immediately covered with Mowiol for same-day imaging. Images were obtained with a Zeiss LSM 710 confocal microscope. Quantitative analyses of lipid droplet size and density were performed using the Image J software with "analyze particles" function in thresholded single images. Sections were taken at similar coordinates in the central brain on an area of 0.05 mm^2. For LD density, data were presented as mean ± SEM from 3 to 5 animals. To measure fluorescence intensities of the FasII staining, maximum intensity projections were generated with confocal stacks imaged using the same parameters. All lobes of mushroom body were defined by a ROI, thresholded and fluorescence intensity measured using Image J. Four to six animals were used per condition.

Histology and transmission electron microscopy

Adult fly heads were embedded as follow for optical and electron microscopy. At least, 3 animals were analyzed for each group. Heads were dissected in cold PBS to remove the proboscis. Heads were fixed in a mixture of 2.5% glutaraldehyde, 2% paraformaldehyde, 5 mM CaCl2, in 0.1 M sodium cacodylate pH7.4 overnight at 4°C. After one rinse in 0.1 M sodium cacodylate during 15 min, heads were post-fixed for 2 h at 4°C in a mixture of 2.5% glutaraldehyde, 0.8% osmium tetroxide in 0.1 M sodium cacodylate. Samples were then rinsed as above in the same buffer, quickly passed through distilled water, and dehydrated through an ascending series of ethanol. Dehydration was completed by 3 bathes of 15 min each in acetone. Heads were then embedded in Epon 812 (Euromedex; France) and resin polymerized at 60°C for 3 days. Blocks were cut with an ultramicrotom (Leica, Ultracut S). Semi-thick 2 µm plastic sections were cut, warm-stained with toluidine blue and observed with a Zeiss Apotome AxioObserver inverted microscope under the control of Axiovision software (Carl Zeiss MicroImaging GmbH). Regions at the level of the antennal lobes in the antero-posterior axis were identified and, on the same blocks, ultrathin 70 nm sections (silver to pale-gold) were cut, collected on copper grids and stained with Reynold's lead citrate for 2 min. They were then observed with a Morgagni 268 transmission electron microscope (Philips, Netherlands).

Reverse transcription-PCR

Ten to fifteen heads of 1-day or 5-day post-eclosion female flies were collected on ice and total RNA was extracted using TRIzol reagent (Invitrogen). Sample concentrations were measured by using a Nanodrop spectrophotometer (Thermo Fisher Scientific). RNA samples were treated with DNase I (Promega) to remove genomic DNA and reverse transcription was performed with Improm-II Reverse Transcriptase (Promega). Total RNA samples for RT-PCR were independently prepared 3 times. Gene-specific transcription levels were monitored by using ABI Prism 7500 Fast thermal cycler (Applied Biosystems, Thermo Fischer Scientific, France) and Fast SYBR Green Master mix (Applied Biosystems). Data were analyzed using the relative quantification method (-2 ΔCt method). The transcript levels were normalized with values obtained after amplification of ribosomal RNA (*rp49*) as endogenous control. Melting curves were established for each reaction to check that only one specific amplicon was synthesized during the amplification. Microsoft Excel software was used to analyze data and to generate graphs expressing mean expression levels ± SEM. Expression levels were presented in percent relative to controls. Results are expressed as -fold change relative to control. The following primers were used for the transcript amplification of the different genes: *ND23* forward: ACCGGCCACTATCAACTATCCCTT; *ND23* reverse: TGACAGAATCCGCAGTAGATGCAC; *PFK* forward: ATGGGTGGCTACTGTGGCTATTTG; *PFK* reverse: TGTAGTTCTCGCTAGCCTTCTCGT; *rp49* forward: CACCAGTCGGATCGATATGCTAA; *rp49* reverse: AATCTCCTTGCGCTTCTTGGAG.

Statistical analysis

All tests were performed with the GraphPad Prism software and $p<0.05$ was considered to be significant. Survival curves were generated by using log-rank test. Two groups of data following a normal distribution were analyzed by unpaired two-sample Student's t-test. Instead, the non-parametric Mann-Whitney test was used when the assumption of normality was not possible. For multiple group comparisons, we used one-way ANOVA followed by Bonferroni's multiple comparison test or Dunnett's test for comparison to the same control. The non-parametric ANOVA was tested when normality of the data was not verified.

RESULTS

Neuronal expression of *ND23* RNAi in flies recapitulates CID features

The expression of transgenic RNAi directed against *ND23* subunit of complex I was achieved using the GAL4/UAS system (Brand and Perrimon, 1993). Since mutations in mitochondrial genes are known to cause early death, we analyzed the effect of complex I knockdown mediated by *ND23* RNAi on *Drosophila* survival. Ubiquitous RNAi knockdown of *ND23* by the driver *actin5C-GAL4* at 19°C led to larval/pupal lethality with no escapers, indicating a critical vital role for this essential subunit. Next, we used the pan-neuronal driver *elav-GAL4* to study the effects of neuronal complex I knockdown in adult fly. In this condition, RT-qPCR experiments revealed that *ND23* RNAi expression resulted in a 75% decrease of brain mRNA level (Fig. 1A). Interestingly, lifespan of flies expressing *ND23* RNAi in neurons was significantly shortened (Fig. 1B) with a mean survival of 30 ± 1.2 days versus 85 ± 1.4 days in control flies. These data indicate that the *ND23* RNAi may directly affect mitochondrial function by decreasing expression of the *ND23* subunits, therefore inducing early death.

To test functional disability, we used negative geotaxis, a commonly used behavioral test in *Drosophila*. We revealed significant motor dysfunction in the neuronal *ND23* knockdown flies 1 day post-eclosion with 58% of flies unable to climb (Fig. 1C). At 4 days, the locomotor performance was strongly reduced since only 1% of knockdown flies were able to climb to the top of the column versus more than 70% of control flies. Most of RNAi flies (78%) remained at the bottom and the others stayed along the column. We conclude that *ND23* knockdown in fly neurons strikingly impairs locomotor activity.

To confirm that the abnormal phenotype of flies expressing *ND23* RNAi in neurons was due to a direct pathological effect on mitochondrial function, we measured brain ATP content. After neuronal knockdown of *ND23*, ATP levels were significantly decreased (-28%) when compared to controls (Fig. 1D). Since the large majority of *Drosophila* brain cells are neurons (Pfrieger and Barres, 1995; Awasaki *et al.*, 2008), we predominantly detected neuronal ATP amounts in the adult fly brain. This may reflect an alteration of the proton gradient due to *ND23* knockdown triggering a decrease in the overall respiratory chain functioning. Together, these data indicate that *ND23* knockdown in neurons causes mitochondrial energy deficits and therefore leads to early fly death and locomotor defects, mirroring features frequently seen in human CID diseases.

Neuronal expression of *ND23* RNAi in flies induces degeneration in the retina and mushroom bodies

Next, we investigated the effect of the expression of *ND23* RNAi in eyes by performing pseudopupil analysis. The well-characterized development of photoreceptor neurons in fly eyes is a powerful model

for analyzing genes contributing to human neurodegenerative diseases. Notably, the eyes of human patients suffering Leigh syndrome are affected with optic atrophy or retinitis pigmentosa (Distelmaier *et al.*, 2009; Assouline *et al.*, 2012). In 1 day-old knockdown flies, the ommatidia presented no obvious defects, and 90% possessed 7 rhabdomeres per ommatidium with the typical trapezoidal organization (Fig. 2A, B). However, in 4 day-old flies, the eyes of the knockdown flies displayed only 5% of normal ommatidia. In the majority of ommatidia, 1 to 6 photoreceptors were missing, leading to aberrant morphological feature of ommatidia (Fig. 2A, B). The neurodegeneration then progressively spread so that, by day 12, photoreceptors became hardly distinguishable (Fig. 2A). These data indicate that neuronal knockdown of *ND23* induces severe and progressive loss of photoreceptor neurons. We also noted that at 20 days of adult life, but not at 4 days, large vacuoles were present in the retina sections in addition to the ommatidia disorganization (Fig. 2C).

To assess whether neurons in the central nervous system were also vulnerable to CID, we performed histological studies on the brain and optic lobes. In the fly brain, the neuronal and glial cell bodies are located in cortical regions, and the neuronal soma and axons are wrapped by glial cell processes. The distinct neuropile regions contain intermingled processes of neurons, glia and synaptic connections. We observed no obvious brain abnormalities using toluidine blue staining on young (4 days) and old (20 days) knockdown animals compared with controls (Fig. 3A-D). In the same manner, the synaptic network downstream of the photoreceptors appeared intact on histological sections of the optic lobes (not shown).

To determine whether the *ND23* RNAi expression in neurons of the fly central brain lead to discrete neuronal loss, we analyzed the structure of mushroom bodies using immunostaining for Fasciclin II (FasII). Mushroom bodies are an associative area into the central brain controlling complex behaviors such as locomotion or learning and memory (Crittenden *et al.*, 1998) and are highly vulnerable in *Drosophila* models of neurodegenerative diseases (Agrawal *et al.*, 2005). Axonal projections of the mushroom body form distinct lobes, which could be evidenced by FasII immunostaining (Pech *et al.*, 2013). As illustrated in Fig. 3E, F, the morphology of the different lobes was conserved. However, immunostaining of FasII was decreased in the mushroom bodies of knockdown brain and this decrease was more pronounced in the γ-lobes relatively to the α- and β-lobes (Fig. 3E, F). Quantification of fluorescence intensity indicated a reduced overall FasII staining in the mushroom bodies of neuronal knockdown flies when compared with controls (Fig. 3G). This may suggest discrete axonal loss caused by the *ND23* RNAi or altered axonal homeostasis.

Glucose transporter overexpression rescues the alterations induced by neuronal *ND23* knockdown

To investigate the impact of cellular metabolism deregulation in the neuropathology, we tested whether the increase in glucose metabolism could be beneficial. Indeed, we previously observed that the overexpression of the human glucose transporter *hGluT3* is able to suppress the lethality induced by the *ND23* RNAi (Besson *et al.*, 2015). We verified that expression of *hGluT3* in the knockdown neurons

rescued almost totally the lethality with a mean survival of 70 days instead of 33 days in *ND23* RNAi flies (Fig. 4A). We further investigated whether increased glucose transporter expression could also restore other deficits. Negative geotaxis test showed that climbing performance was significantly rescued (Fig. 4B), the locomotor performances of flies co-expressing *ND23* RNAi and *hGluT3* being similar to that of controls. Pseudopupil analysis of 4 day-old flies co-expressing *ND23* RNAi and *hGluT3* showed that 78% ommatidia possessed a typical architecture with 7 rhabdomeres versus 5% in knockdown flies (Fig. 4C). However, at 20 days after adult emergence, only 5% ommatidia contained 7 photoreceptors in flies co-expressing *ND23* RNAi and *hGluT*3 indicating that the rescue was transient. Finally, we found that overexpression of *hGluT3* in neuronal knockdown fly heads restored ATP at the same level than in control flies (Fig. 4D). These data suggest that increasing glucose transport might enhance glycolysis and compensate for ATP depletion in *ND23* knockdown flies. To test this hypothesis, we investigated whether the rate-limiting enzyme of glycolysis, the phosphofructokinase (*PFK*), may have a beneficial effect (Tennessen *et al.*, 2011). We showed that overexpressed *PFK* transcript levels were significantly increased (with a 3-fold increase as analyzed by RT-qPCR) versus the endogenous *PFK* level in neuronal knockdown flies (Fig. 5A). Moreover, the endogenous *PFK* levels were not statistically different in neuronal knockdown flies in the presence or absence of the *hGluT3* transgene (Fig. 5A). The survival of the *PFK* overexpressing-flies (mean survival of 32.5 days) did not increase when compared to *ND23* RNAi flies (Fig. 5B) and *PFK* overexpression did not rescue the photoreceptor loss in the eyes (Fig. 5C-D). In conclusion, enhancing glucose metabolism by increasing glucose up-take in *ND23* knockdown flies rescues neuronal alterations by a mechanism which might be independent of glycolysis.

***ND23* knockdown in glia induces a degenerative phenotype**

Since glial alterations are known to promote neurodegeneration in several disorders (Lobsiger and Cleveland, 2007; Colodner and Feany, 2010), we investigated whether glial complex I deficiency could play a role in CID. We used *repo-GAL4* as a glial driver to express *ND23* RNAi in all types of glial cells.

We first performed histological studies on brain sections stained with toluidine blue. In contrast to the results obtained with the neuronal driver, we observed a massive vacuolization throughout the cortical regions of the brain and optic lobes at 4 days of the adult life (Fig. 6B1, B2). Vacuoles with contents presenting different staining intensities by toluidine blue were observed in the brain of 20 day-old glial knockdown flies (Fig. 6E1, E2). In addition, we noted many dark spheroid deposits at the border of the cortex and the neuropile, suggesting the presence of LDs (Fig. 6B2). At 20 days, these deposits were also found within neuropile structures (Fig. 6E1, E2). The abnormal brain morphology of the glial-induced *ND23* RNAi flies prompted us to investigate whether this neurodegenerative feature led to altered survival or behavior in these animals. The longevity was nearly the same in knockdown and control flies (Fig. 6F) that displayed a mean survival of 79 days and 84 days, respectively. Climbing assays indicated no significant difference in locomotion performance at 12 days (Fig. 6G), with 56% of control and 49% of knockdown flies having reached the top of the column. Intriguingly, these data showed that, while the

glial-specific *ND23* knockdown causes severe damage in the fly brain, it does not lead to a significant behavioral dysfunction, in contrast to the phenotype induced by neuronal specific knockdown.

_ND23_ knockdown in glia induces perturbation of lipid metabolism homeostasis with lipid droplet accumulation

To determine whether the dark spheroid deposits observed on toluidine blue sections were LDs, we performed neutral lipid staining with Nile Red (not shown) or Bodipy on dissected fly brains that were imaged by confocal microscopy. In control animals, we observed few LDs scattered throughout the cortical areas of the brain, where neuron and glia soma are located (Fig. 7A1-A3), as described by Kis *et al.* (2015). In the brain of *ND23* RNAi-expressing glia, we observed that LDs were much more numerous than in controls and massively accumulated at the cortex-neuropile boundary (Fig. 7B1-B3). Strikingly, at 4 days, glia expressing *ND23* RNAi elicited approximately a 5-fold increase in the number of LDs (Fig. 7D). Moreover, the LDs displayed larger size in glial ND23 knockdown flies than in controls (compare Fig. B3 with A3). Although most of the LDs had an area less than 3 μm^2 in controls (69 %), larger LDs were frequently found in *ND23* RNAi-expressing glia (63% with an area > 3 μm^2) (Fig. 7E). This strong increase in the size of LDs in the brain of flies with glial *ND23* RNAi expression suggests that LDs may grow by the concomitant addition of phosholipids at the LD surface and triacylglecerols within the core or they may tend to fuse together.

Next, we examined the localization of ectopic EYFP-tagged perilipin-2, a protein specifically located at the LD monolayer membrane (Bi *et al.*, 2012; Kühnlein, 2011; Miura *et al.*, 2002). Using the glial driver *repo*, we found that immunofluorescence for YFP revealing perilipin-2 was localized as a coat of LDs in the brain (Fig. 7F1, F2). In flies expressing *ND23* RNAi in glia, the perilipin-2 positive LDs were much more abundant (Fig. 7G1, G2) with a similar distribution pattern than that obtained with Bodipy staining. These data are in accordance with the distribution of perilipin-2 in the region of cortex glia (Kis *et al.*, 2015). Using the neuronal driver *elav*, perilipin-2 was faintly detected in control flies (Fig. 7H) and in flies expressing *ND23* RNAi (Fig. 7I). In conclusion, we showed using two lipid probes Nile Red and Bodipy a strong accumulation of LDs induced by glial ND23 knockdown cells and we demonstrated that the LDs are located in glial cells using ectopic perilipin-2 expression under the control of the glial driver *repo*. These data indicate that lipid metabolic pathways are altered in relation with mitochondrial dysfunction in glial cells.

Ultrastructural analysis of brain with neurons or glia expressing _ND23_ RNAi

Next, we examined at the ultrastructural level the brain alterations induced by complex I deficiency in neuronal or glial cells. In control brain (*elav>*w^{1118} and *repo>*w^{1118} genotypes), the neuronal soma were tightly enveloped by glial cell processes identified by their high electron density (Fig. 8A, C, arrows). Electron microscopy analysis revealed that neuronal ND23 knockdown brain had normal morphology compared to control (Fig. 8B). In glial knockdown brain, we observed the presence of numerous vacuoles

throughout the cortical regions (Fig. 8D1 and D3) whereas control brain did not exhibit any discernible vacuoles (Fig. 8C). These vacuoles presented various sizes and aspects on the same section. Some vacuole contents appeared empty while others were filled with a scarce material (Fig. 8D1). The morphology of the neuronal cell bodies appeared normal, tightly enveloped by glial cell processes (Fig. 8D1). As illustrated in Fig. 8D3, we observed numerous LDs presenting darkly homogenous bodies, predominantly localized at the border between the cortex and neuropile. As expected, LDs were seen in the cytoplasm of glial cells (Fig. 8D1, D3), which present electron-dense nuclei and cytoplasmic processes (Buchanan and Benzer, 1993). We observed that 85% of LDs were unambiguously localized in glial cells, 1% in neurons, and 14% were not clearly attributed to any cell type in the vicinity of neuronal soma or processes (3 brains, 50 images, 97 LDs). These LDs were sometimes associated with mitochondria (Fig. 8D2) or with vacuoles (Fig. 8D3). In conclusion, we propose that glial downregulation of *ND23* causes abnormal formation of vacuoles and LDs, which leads to the degenerative phenotype in these flies.

Glucose transporter overexpression does not rescue the degenerative phenotype induced by glial *ND23* knockdown

Having observed that the *hGluT3* overexpression rescues the lethality and locomotor defects induced by complex I deficiency in neurons, we tested whether it may also have a beneficial effect in glial cells. We still observed an intense vacuolization in the brain of flies expressing *hGluT3* (*repo>ND23* RNAi; *hGluT3* genotype) on semi-thin sections (Fig. 6C1, C2). We noticed that LDs accumulated as dark puncta at the border with the neuropile (Fig. 6C2) as observed in glial ND23 knockdown (Fig. 6B2). Using Bodipy staining, we observed that LDs accumulated in the brain overexpressing *hGluT3* in glia (Fig. 7C1-C3). Their density and size were similar to that of *repo>ND23* RNAi (Fig. 7D, E). Thus, increasing glucose up-take does not rescue the neurodegenerative phenotype associated with glial knockdown of *ND23*.

DISCUSSION

In this study, we show that knockdown of *ND23,* the homologue of *NDUFS8,* in *Drosophila* brain recapitulates key features of mitochondrial diseases, with contributions of neurons and glial cells to disease pathogenesis. We demonstrate that neuronal knockdown of *ND23* critically reduces locomotion behavior and lifespan associated with decreased ATP levels. All these phenotypes are rescued by the overexpression of glucose transporter. We did not observe massive neuronal loss but progressive neuronal degeneration of photoreceptors and alterations in discrete brain structures such as the mushroom bodies. Thus, neuronal loss is restricted to some brain areas as it is the case in human mitochondrial encephalopathies (Assouline *et al.*, 2012). Moreover, we provide evidence that the partial loss of *ND23* specifically in glial cells contributes to the mitochondrial pathogenesis. Indeed, degenerative vacuoles and numerous LDs are invading the brain of glial knockdown flies although they display normal behavior. Thus, we show that *ND23* RNAi induces different pathways of toxicity in these two cell types and that overall cell homeostasis is profoundly disturbed by the complex I knockdown. Our results bring new evidence that neurodegeneration in CID may be strongly influenced by an alteration of glial homeostasis, in particular with accumulation of lipid droplets, that may affect the vulnerable neurons in the central brain. In agreement with our observations, two recent reports have shown that glial cells are critically implicated in *Drosophila* models of complex I subunit loss (Hegde *et al*. 2014; Liu *et al.* 2015).

We show that ATP production is decreased by 28% in neuronal knockdown brain. At first glance, this decrease does not involve immediate and irreversible damage in the brain and seems to be in the same range than that described in other fly and mouse CID models (Leong *et al.*, 2012; Burman *et al.*, 2014). Mutation of complex I may induce a compensatory up-regulation of the complex II-dependent respiratory capacity as analyzed by microarrays in *C. elegans* and human (Crimi *et al.*, 2005; Falk *et al.*, 2009). Intriguingly, the inability to produce high amounts of ATP in neurons, inducing cumulative detrimental effects, is reversed by genetic manipulation of *hGluT3*. However, this rescue by glucose entry may not be mediated by an up-regulation of the glycolysis which is dispensable in neurons (Halim *et al.*, 2010; Volkenhoff *et al.*, 2015). It is known that glucose metabolic disturbances are implicated in neurodegenerative disease progression (Senatorov et al, 2003; Ding *et al.*, 2013). As suggested by studies in mice or flies, cells with defective mitochondria could shift from metabolic activity of the respiratory chain to other types of energetic pathways. They use fatty acid β-oxidation, glycolysis or protein catabolism due to transcriptional dysregulation of genes affecting the diverse metabolic processes (Crimi *et al.*, 2005; Fernandez-Ayala *et al.*, 2010; Celotto *et al.*, 2011). Indeed, metabolomic analysis of mitochondrial disease models associated with cytochrome oxidase deficiency (Vartiainen *et al.*, 2014; Kemppainen *et al.*, 2016), or ATP synthase mutation (Celotto *et al.*, 2011) that are impacting respiratory

complexes shows a switch to glycolysis for ATP production. In *ND23* knockdown, the increased glucose entry due to transporter overexpression may likely trigger a compensatory metabolic pathway. We show that overexpression of the glycolysis rate-limiting enzyme *PFK* has no effect on survival or photoreceptor degeneration. However, activation of enzymes downstream of *PFK*, as reported by Nirala *et al.* (2013) may be activated by glucose entry in *ND23* knockdown flies to promote glycolysis. Finally, although the precise mechanisms involved remain difficult to establish because of the complex interplay between the different metabolic pathways, we have identified enhancement of the glucose transporter as a potential therapeutic strategy to compensate mitochondrial dysfunction in CID. With this respect, it is interesting to note that the glucose transporters GluT1 and GluT3 have been reported to be impaired in neurodegenerative diseases such as Huntington's disease (Morea *et al.*, 2017) or Alzheimer 's disease (Mark *et al.*, 1997; Shah *et al.*, 2012). More precisely, increased glucose transport is able to rescue a *Drosophila* model of Aβ toxicity (Niccoli *et al*., 2016).

In contrast to neuronal knockdown, glial-specific *ND23* knockdown does not lead to early lethality or behavioral dysfunction but strongly affects nervous system integrity. Strikingly, *ND23* RNAi in glia induces high accumulation of LDs and intense vacuolization. The presence of LDs as neutral lipid storing structures was demonstrated by using two lipophilic dyes Bodipy and Nile Red. In addition, perilipin-2 experiments showed that LDs are located in glial cells as confirmed by ultrastructural analysis. Importantly, we did not observe any LD accumulation in glia resulting from the neuronal knockdown of *ND23*, indicating that LD accumulation results from a cell-autonomous mechanism. In normal conditions, the primary function of LDs is to store triacylglycerols and sterol derivatives, which can be mobilized to fuel ß-oxidation for energy generation and to provide membrane precursors (Goodman, 2009; Guo *et al.*, 2009). From recent investigations (Barbosa and Siniossoglou, 2017), LDs are not seen as simple cytosolic structures that passively store triacylglycerides, but they are at the center of lipid metabolism by interacting with several intracellular organelles including mitochondria. Increased number of LDs has been shown in experimental models of cellular stress such as nutrient deprivation (Cabodevilla *et al*, 2013) and in metabolic or mitochondrial diseases (Greenberg *et al.*, 2011; Bayat *et al.*, 2012; Golla *et al.*, 2017). In flies, excessive LD levels were detected as signs of disturbed lipid metabolism in several models of mitochondrial dysfunction (Navarro *et al.*, 2010; Kishita *et al.*, 2012; Schulz *et al.*, 2015). In the report of Liu *et al* (2015), knockdown of the *ND42* complex I subunit has been shown to induce LD accumulation in glia prior to or at the onset of photoreceptor neurodegeneration as a non-cell autonomous process and may represent an indicator and a promoter of neurodegeneration. In the central brain, we show here that knockdown of the *ND23* complex I subunit results in cell-autonomous accumulation of LDs in glial cells. We hypothesize that in our model of defective mitochondria, conversion of fatty acids through β-oxidation, which occurs only in glial cells (Schulz *et al*., 2015), might be impaired or delayed. Consequently, LDs accumulate because the free fatty acids are not degraded by mitochondria, whereas in wild-type animals LDs are known to undergo a rapid turnover. With this respect, we observed some LDs

directly associated with mitochondria. The lipid over-loading may overwhelm the metabolic machinery by exceeding the storage capacity of the cell, and the excess of LDs may become toxic inducing vacuolization of glial cells. Using electron microscopy, we show that numerous LDs are in contact with vacuoles, some unambiguously localized within glial cells. On the other hand, it has been described that accumulation of excess fatty acids in cellular triacylglyceride stores may be protective against lipotoxicity (Listenberger *et al.*, 2003; Logan-Garbisch *et al.*, 2014). Moreover, from our analysis, it seems that triacylglycerides accumulated into LDs are unsaturated lipids due to their high affinity for osmium tetroxide (De Martino *et al.*, 1968; Digel *et al.*, 2010; Fujimoto *et al.*, 2013). In our conditions, the LDs appear as dark homogenous bodies, although they have often reported as grayish round structures (Kis *et al.,* 2015). This variability in the electron density of the LD content may be explained by sample preparation but also by the nature of internalized lipids (Fujimoto and Parton, 2011; Fujimoto *et al.*, 2013). Thus, we hypothesize that the darkness of LDs in glial *ND23* knockdown brains might indicate a lipid composition different from the LDs described by Kis *et al*. (2015) in wild-type *Drosophila* brain, possibly reflecting a different metabolic state. Unsaturated lipids located into the LDs could be protected from peroxidation reactions. Indeed, the LD core could provide a protective environment that reduces peroxidation of unsaturated fatty acids to limit oxidative damages. Such a role of LDs has been described by Herms *et al.* (2013) and also reported in *Drosophila* for protecting glial cells but also neighboring neuroblasts (Bailey *et al*, 2015). Therefore, the glial LDs induced by mitochondrial alteration may reflect a compensatory mechanism.

Glial *ND23* knockdown induces the formation of numerous vacuoles that were mainly observed in the brain cortical regions, which house cortex glial cells and neuronal cell bodies (Hartenstein, 2011). This could be related to the specific function of cortex glia or to their increased susceptibility to mitochondria dysfunction compared to the other glial cell types. As glia display phagocytic function (Doherty *et al.*, 2009), we hypothesize that *ND23* RNAi-expressing cortex glial cells may also phagocyte neighboring neurons becoming dysfunctional. Vacuoles are not detected in the brain of neuronal *ND23* knockdown, indicating that their presence is specific to the expression of glial *ND23* RNAi. Moreover, we never observed fragmented nuclei nor cytoplasm lysis indicative of cell death and no phagophore formation allowing autophagy to proceed. In semi-thin sections, all vacuoles have a clear content in young flies, but some vacuoles appear filled with amorphous substrate at 20 days. This is consistent with electron microscopy analysis, which reveals variably sized vacuoles delineated by a single monolayer membrane, containing scarce electron-dense material or undigested membrane debris. Such vacuoles have been described in a variety of *Drosophila* mutants associated with neurodegeneration (Buchanan and Benzer, 1993; Min and Benzer, 1997; Mühlig-Versen *et al.*, 2005; Dutta *et al.*, 2015; Sivachenko *et al.,* 2016). This strengthens the concept of the conserved nature of degenerative pathways between diverse genotypes. Recent reports point out that interacting degenerative pathways are induced in neurons and glia using different *Drosophila* models of CID, including knockdown for *ND75*, the homologue of

NDUFS1 and *ND42,* the homologue of *NDUFA10* (Hegde *et al.*, 2014; Liu *et al.* 2015). Strikingly, we show that, using cell-type specific *ND23* knockdown, behavioral alteration and organismal toxicity are not correlated with histological features of neurodegeneration such as vacuolization or accumulation of LDs and vice versa. In addition, overexpression of the human glucose transporter *hGluT3* is able to rescue the lethality and locomotor defects induced by CID in neurons, whereas it has no effect on vacuolization and accumulation of lipid droplets in glial cells. The link between increased lipid amounts and CID is still elusive and therefore, whether the formation of LDs in glia may have a protective role or actively participate to neurodegeneration in CID deserves further careful investigations.

Acknowledgments

We thank Dr C.S. Thummel and Dr R.P. Kühnlein for the generous gift of flies carrying PFK and YFP-tagged perilipin-2, respectively. We also thank the Bloomington *Drosophila* Stock Center and the Vienna *Drosophila* RNAi Center for transgenic flies, and the Developmental Studies Hybridoma Bank (DSHB) for antibodies. The authors are grateful to Marie-Pierre Blanchard for her expertise in confocal analysis, and to Aïcha Aouane, Nicolas Brouilly and Fabrice Richard for their support in electron microscopy analysis.

References

Agrawal, N., Pallos, J., Slepko, N., Apostol, B. L., Bodai, L., Chang, L. W., . . . Marsh, J. L. (2005) Identification of combinatorial drug regimens for treatment of Huntington's disease using *Drosophila. Proceedings of the National Academy of Sciences,102*(10), 3777-3781.

Assouline, Z., Jambou, M., Rio, M., Bole-Feysot, C., Lonlay, P. D., Barnerias, C., . . . Lebre, A. (2012). A constant and similar assembly defect of mitochondrial respiratory chain complex I allows rapid identification of NDUFS4 mutations in patients with Leigh syndrome. *Biochimica et Biophysica Acta (BBA) - Molecular Basis of Disease, 1822*(6), 1062-1069.

Awasaki, T., Lai, S., Ito, K., & Lee, T. (2008). Organization and postembryonic development of glial cells in the adult central brain of *Drosophila*. *Journal of Neuroscience, 28*(51), 13742-13753.

Bailey, A., Koster, G., Guillermier, C., Hirst, E., Macrae, J., Lechene, C., . . . Gould, A. (2015). Antioxidant role for lipid droplets in a stem cell niche of *Drosophila*. *Cell, 163*(2), 340-353.

Barbosa, A. D., & Siniossoglou, S. (2017). Function of lipid droplet-organelle interactions in lipid homeostasis. *Biochimica et Biophysica Acta (BBA) - Molecular Cell Research*, 1864(9), 1459-1468

Bayat, V., Thiffault, I., Jaiswal, M., Tétreault, M., Donti, T., Sasarman, F., . . . Bellen, H. J. (2012). mutations in the mitochondrial methionyl-trna synthetase cause a neurodegenerative phenotype in flies and a recessive ataxia (ARSAL) in humans. *PLoS Biology, 10*(3), e1001288.

Besson, M. T., Alegría, K., Garrido-Gerter, P., Barros, L. F., & Liévens, J. (2015). Enhanced Neuronal Glucose Transporter Expression Reveals Metabolic Choice in a HD *Drosophila* Model. *Plos One, 10*(3), e0118765.

Bi, J., Xiang, Y., Chen, H., Liu, Z., Gronke, S., Kuhnlein, R. P., & Huang, X. (2012). Opposite and redundant roles of the two *Drosophila* perilipins in lipid mobilization. *Journal of Cell Science, 125*(15), 3568-3577.

Brand, A.H. & Perrimon, N. (1993). Targeted gene expression as a means of altering cell fates and generating dominant phenotypes. *Development., 118*(2), 401-415.

Buchanan, R. L., & Benzer, S. (1993). Defective glia in the *Drosophila* brain degeneration mutant *drop-dead*. *Neuron, 10*(5), 839-850.

Burman, J. L., Itsara, L. S., Kayser, E., Suthammarak, W., Wang, A. M., Kaeberlein, M., . . . Pallanck, L. J. (2014). A *Drosophila* model of mitochondrial disease caused by a complex I mutation that uncouples proton pumping from electron transfer. *Disease Models & Mechanisms, 7*(10), 1165-1174.

Cabodevilla, A. G., Sánchez-Caballero, L., Nintou, E., Boiadjieva, V. G., Picatoste, F., Gubern, A., & Claro, E. (2013). Cell survival during complete nutrient deprivation depends on lipid droplet-fueled β-oxidation of fatty acids. *Journal of Biological Chemistry, 288*(39), 27777-27788.

Celotto, A. M., Chiu, W. K., Voorhies, W. V., & Palladino, M. J. (2011). Modes of Metabolic Compensation during Mitochondrial Disease Using the *Drosophila* Model of ATP6 Dysfunction. *PLoS ONE, 6*(10), e0025823

Colodner, K. J., & Feany, M. B. (2010). Glial Fibrillary Tangles and JAK/STAT-Mediated Glial and Neuronal Cell Death in a *Drosophila* Model of Glial Tauopathy. *Journal of Neuroscience, 30*(48), 16102-16113.

Crimi, M., O'Hearn, S. F., Wallace, D. C. & Comi, G. P.. (2005). Molecular Research Technologies in Mitochondrial Diseases: The Microarray Approach. *IUBMB Life,* 811- 818.

Crittenden, J. R., Skoulakis, E. M., Han, K. A., Kalderon, D. & Davis, R. L. (1998). Tripartite mushroom body architecture revealed by antigenic markers. *Learning & Memory, 5*(1-2),38-51.

De Martino, C., Natali, P. G., Bruni, C. B., & Accinni, L. (1968). Influence of plastic embedding media on staining and morphology of lipid bodies. *Histochemie, 16*(4), 350-360.

Digel, M., Ehehalt, R., & Füllekrug, J. (2010). Lipid droplets lighting up: Insights from live microscopy. *FEBS Letters, 584*(11), 2168-2175.

Ding, F., Yao, J., Rettberg, J. R., Chen, S., & Brinton, R. D. (2013). Early decline in glucose transport and metabolism precedes shift to ketogenic system in female aging and Alzheimer's mouse brain: Implication for bioenergetic intervention. *PLoS ONE, 8*(11), e0079977.

Distelmaier, F., Koopman, W. J., Heuvel, L. P., Rodenburg, R. J., Mayatepek, E., Willems, P. H., & Smeitink, J. A. (2009). Mitochondrial complex I deficiency: from organelle dysfunction to clinical disease. *Brain, 132*(4), 833-842.

Doherty, J., Logan, M. A., Tasdemir, O. E., & Freeman, M. R. (2009). Ensheathing glia function as phagocytes in the adult *Drosophila* brain. *Journal of Neuroscience, 29*(15), 4768-4781.

Dutta, S., Rieche, F., Eckl, N., Duch, C., & Kretzschmar, D. (2015). Glial expression of Swiss cheese (SWS), the *Drosophila* orthologue of neuropathy target esterase (NTE), is required for neuronal ensheathment and function. *Disease Models & Mechanisms, 9*(3), 283-294.

Falk, M. J., Rosenjack, J. R., Polyak, E., Suthammarak, W., Chen, Z., Morgan, P. G., & Sedensky, M. M. (2009). Subcomplex Iλ specifically controls integrated mitochondrial functions in *Caenorhabditis elegans*. *PLoS ONE, 4*(8), e0006607.

Fassone, E., & Rahman, S. (2012). Complex I deficiency: clinical features, biochemistry and molecular genetics. *Journal of Medical Genetics, 49*(9), 578-590.

Fernández-Ayala, D. J., Chen, S., Kemppainen, E., Odell, K. M., & Jacobs, H. T. (2010). Gene expression in a *Drosophila* model of mitochondrial disease. *PLoS ONE, 5*(1), e0008549.

Franceschini, N. & Kirschfeld, K. (1971). Pseudopupil phenomena in the compound eye of drosophila. *Kybernetik., 9*, 159–182.

Gerards, M., Sallevelt, S. C., & Smeets, H. J. (2016). Leigh syndrome: Resolving the clinical and genetic heterogeneity paves the way for treatment options. *Molecular Genetics and Metabolism, 117*(3), 300-312.

Golla, S., Ren, J., Malloy, C. R., & Pascual, J. M. (2017). Intramyocellular lipid excess in the mitochondrial disorder MELAS. *Neurology Genetics, 3*(3), 1-4.

Goodman, J. M. (2009). Demonstrated and inferred metabolism associated with cytosolic lipid droplets. *Journal of Lipid Research, 50*(11), 2148-2156.

Greenberg, A. S., Coleman, R. A., Kraemer, F. B., McManaman, J. L., Obin, M. S., Puri, V., . . . Mashek, D. G. (2011). The role of lipid droplets in metabolic disease in rodents and humans. *Journal of Clinical Investigation, 121*(6), 2102-2110.

Greenspan, P., Mayer, E. P., & Fowler, S. D. (1985). Nile red: a selective fluorescent stain for intracellular lipid droplets. *The Journal of Cell Biology, 100*(3), 965-973.

Guo, Y., Cordes, K. R., Farese, R. V., & Walther, T. C. (2009). Lipid droplets at a glance. *Journal of Cell Science, 122*(6), 749-752.

Halim, N. D., Mcfate, T., Mohyeldin, A., Okagaki, P., Korotchkina, L. G., Patel, M. S., . . . Verma, A. (2010). Phosphorylation status of pyruvate dehydrogenase distinguishes metabolic phenotypes of cultured rat brain astrocytes and neurons. *Glia*, 58(10),1168–1176.

Hartenstein, V. (2011). Structure and development of glia in *Drosophila*. *Glia, 59*(9), 1237-1252.

Hegde, V.R., Vogel, R. & Feany, M.B. (2014). Glia are critical for the neuropathology of complex I deficiency in *Drosophila*. *Human Molecular Genetics, 23*(17),4686-4692.

Herms, A., Bosch, M., Ariotti, N., Reddy, B., Fajardo, A., Fernández-Vidal, A., . . . Pol, A. (2013). Cell-to-cell heterogeneity in lipid droplets suggests a mechanism to reduce lipotoxicity. *Current Biology, 23*(15), 1489-1496.

Fujimoto, T., & Parton, R. G. (2011). Not Just Fat: The Structure and Function of the Lipid Droplet. *Cold Spring Harbor Perspectives in Biology, 3*(3), a004838.

Fujimoto, T., Ohsaki, Y., Suzuki, M., & Cheng, J. (2013). Imaging Lipid Droplets by Electron Microscopy. *Methods in Cell Biology Lipid Droplets,* 227-251.

Kemppainen, E., George, J., Garipler, G., Tuomela, T., Kiviranta, E., Soga, T., . . . Jacobs, H. T. (2016). Mitochondrial dysfunction plus high-sugar diet provokes a metabolic crisis that inhibits growth. *Plos One, 11*(1), e0145836.

Kis, V., Barti, B., Lippai, M., & Sass, M. (2015). Specialized cortex glial cells accumulate lipid droplets in *Drosophila melanogaster*. *Plos One, 10*(7), e0131250.

Kishita, Y., Tsuda, M., & Aigaki, T. (2012). Impaired fatty acid oxidation in a *Drosophila* model of mitochondrial trifunctional protein (MTP) deficiency. *Biochemical and Biophysical Research Communications, 419*(2), 344-349.

Koopman, W. J., Distelmaier, F., Smeitink, J. A., & Willems, P. H. (2012). OXPHOS mutations and neurodegeneration. *The EMBO Journal, 32*(1), 9-29.

Kühnlein, R. P. (2011). The contribution of the *Drosophila* model to lipid droplet research. *Progress in Lipid Research, 50*(4), 348-356.

Lee, J. S., Kim, H., Lim, B. C., Hwang, H., Choi, J., Kim, K. J., . . . Chae, J. (2016). Leigh Syndrome in Childhood: Neurologic Progression and Functional Outcome. *Journal of Clinical Neurology, 12*(2), 181.

Leigh, D. (1951). Subacute necrotizing encephalomyelopathy in an infant. *Journal of Neurology, Neurosurgery & Psychiatry, 14*(3), 216-221.

Leong, D. W., Komen, J. C., Hewitt, C. A., Arnaud, E., Mckenzie, M., Phipson, B., . . . Scott, H. S. (2012). Proteomic and metabolomic analyses of mitochondrial complex i-deficient mouse model generated by spontaneous B2 Short Interspersed Nuclear Element (SINE) insertion into NADH dehydrogenase (Ubiquinone) Fe-S protein 4 (Ndufs4) gene. *Journal of Biological Chemistry, 287*(24), 20652-20663.

Listenberger, L. L., Han, X., Lewis, S. E., Cases, S., Farese, R. V., Ory, D. S., & Schaffer, J. E. (2003). Triglyceride accumulation protects against fatty acid-induced lipotoxicity. *Proceedings of the National Academy of Sciences, 100*(6), 3077-3082.

Listenberger, L. L., & Brown, D. A. (2007). Fluorescent detection of lipid droplets and associated proteins. *Current Protocols in Cell Biology*, Chapter 24: Unit 24.2.

Liu, L., Zhang, K., Sandoval, H., Yamamoto, S., Jaiswal, M., Sanz, E., . . . Bellen, H. (2015). Glial lipid droplets and ROS induced by mitochondrial defects promote neurodegeneration. *Cell, 160*(1-2), 177-190.

Lobsiger, C. S., & Cleveland, D. W. (2007). Glial cells as intrinsic components of non-cell-autonomous neurodegenerative disease. *Nature Neuroscience, 10*(11), 1355-1360.

Loeffen, J., Smeitink, J., Triepels, R., Smeets, R., Schuelke, M., Sengers, R., . . . Heuvel, L. V. (1998). The first nuclear-encoded complex I mutation in a patient with Leigh syndrome. *The American Journal of Human Genetics, 63*(6), 1598-1608.

Logan-Garbisch, T., Bortolazzo, A., Luu, P., Ford, A., Do, D., Khodabakhshi, P., & French, R. L. (2014). Developmental ethanol exposure leads to dysregulation of lipid metabolism and oxidative stress in *Drosophila*. *G3 (Bethesda), 5*(1), 49-59.

Mark, R. J., Pang, Z., Geddes, J. W., Uchida, K., & Mattson, M.P. (1997). Amyloid beta-peptide impairs glucose transport in hippocampal and cortical neurons: involvement of membrane lipid peroxidation. *Journal of Neuroscience, 17*(3):1046-54.

Min, K., & Benzer, S. (1997). *Spongecake* and *eggroll*: two hereditary diseases in *Drosophila* resemble patterns of human brain degeneration. *Current Biology, 7*(11), 885-888.

Miura, S., Gan, J., Brzostowski, J., Parisi, M. J., Schultz, C. J., Londos, C., . . . Kimmel, A. R. (2002). Functional conservation for lipid storage droplet association among Perilipin, ADRP, and TIP47 (PAT)-related proteins in mammals, *Drosophila*, and *Dictyostelium*. *Journal of Biological Chemistry, 277*(35), 32253-32257.

Morea, V., Bidollari, E., Colotti, G., Fiorillo, A., Rosati, J., Filippis, L. D., . . . Ilari, A. (2017). Glucose transportation in the brain and its impairment in Huntington disease: one more shade of the energetic metabolism failure? *Amino Acids, 49*(7), 1147-1157.

Mühlig-Versen, M., da Cruz, A. B., Tschäpe, J. A., Moser, M., Büttner, R., Athenstaedt, K., . . . Kretzschmar, D. (2005). Loss of Swiss Cheese/Neuropathy Target Esterase activity causes disruption of phosphatidylcholine homeostasis and neuronal and glial death in adult *Drosophila*. *Journal of Neuroscience, 25*(11), 2865-2873.

Navarro, J. A., Ohmann, E., Sanchez, D., Botella, J. A., Liebisch, G., Molto, M. D., . . . Schneuwly, S. (2010). Altered lipid metabolism in a *Drosophila* model of Friedreichs ataxia. *Human Molecular Genetics, 19*(14), 2828-2840.

Niccoli, T., Cabecinha, M., Tillmann, A., Kerr, F., Wong, C., Cardenes, D., . . . Partridge, L. (2016). Increased glucose transport into neurons rescues Aβ toxicity in *Drosophila*. *Current Biology, 26*(17), 2291-2300.

Nirala, N. K., Rahman, M., Walls, S. M., Singh, A., Zhu, L. J., Bamba, T., . . . Acharya, U. R. (2013). Survival response to increased ceramide involves metabolic adaptation through novel regulators of glycolysis and lipolysis. *PLoS Genetics, 9*(6), e1003556.

Pech, U., Dipt, S., Barth, J., Singh, P., Jauch, M., Thum, A. S., . . . Riemensperger, T. (2013). Mushroom body miscellanea: transgenic *Drosophila* strains expressing anatomical and physiological sensor proteins in Kenyon cells. *Frontiers in Neural Circuits, 7*, 147.

Pfrieger, F. W., & Barres, B. A. (1995). What the flys glia tell the flys brain. *Cell, 83*(5), 671-674.

Porcelli, D., Barsanti, P., Pesole, G., & Caggese, C. (2007). The nuclear OXPHOS genes in insecta: a common evolutionary origin, a common cis-regulatory motif, a common destiny for gene duplicates. *BMC Evolutionary Biology, 7*(1), 215.

Procaccio, V., Depetris, D., Soularue, P., Mattei, M., Lunardi, J., & Issartel, J. (1997). cDNA sequence and chromosomal localization of the NDUFS8 human gene coding for the 23 kDa subunit of the mitochondrial complex I. *Biochimica et Biophysica Acta (BBA) - Gene Structure and Expression, 1351*(1-2), 37-41.

Rahman, S., Blok, R. B., Dahl, H. M., Danks, D. M., Kirby, D. M., Chow, C. W., . . . Thorburn, D. R. (1996). Leigh syndrome: Clinical features and biochemical and DNA abnormalities. *Annals of Neurology, 39*(3), 343-351.

Rodenburg, R. J. (2016). Mitochondrial complex I-linked disease. *Biochimica et Biophysica Acta (BBA) - Bioenergetics, 1857*(7), 938-945.

Schulz, J. G., Laranjeira, A., Huffel, L. V., Gärtner, A., Vilain, S., Bastianen, J., . . . Dotti, C. G. (2015). Glial β-oxidation regulates *Drosophila* energy metabolism. *Scientific Reports, 5*(1), 7805.

Senatorov, V. V., Charles, V., Reddy, P., Tagle, D. A., & Chuang, D. (2003). Overexpression and nuclear accumulation of glyceraldehyde-3-phosphate dehydrogenase in a transgenic mouse model of Huntington's disease. *Molecular and Cellular Neuroscience, 22*(3), 285-297.

Shah, K., Desilva, S., & Abbruscato, T. (2012). The Role of Glucose Transporters in Brain Disease: Diabetes and Alzheimer's Disease. *International Journal of Molecular Sciences, 13*(12), 12629-12655.

Sivachenko, A., Gordon, H. B., Kimball, S. S., Gavin, E. J., Bonkowsky, J. L., & Letsou, A. (2016). Neurodegeneration in a *Drosophila* model of adrenoleukodystrophy: the roles of the Bubblegum and Double bubble acyl-CoA synthetases. *Disease Models & Mechanisms, 9*(4), 377-387.

Tennessen, J. M., Baker, K. D., Lam, G., Evans, J., & Thummel, C. S. (2011). The *Drosophila* estrogen-related receptor directs a metabolic switch that supports developmental growth. *Cell Metabolism, 13*(2), 139-148.

Vartiainen, S., Chen, S., George, J., Tuomela, T., Luoto, K. R., Odell, K. M., & Jacobs, H. T. (2014). Phenotypic rescue of a *Drosophila* model of mitochondrial ANT1 disease. *Disease Models & Mechanisms, 7*(6), 635-648.

Vinothkumar, K. R., Zhu, J., & Hirst, J. (2014). Architecture of mammalian respiratory complex I. *Nature, 515*(7525), 80-84.

Volkenhoff, A., Weiler, A., Letzel, M., Stehling, M., Klämbt, C., & Schirmeier, S. (2015). Glial glycolysis is essential for neuronal survival in *Drosophila*. *Cell Metabolism, 22*(3), 437-447.

Wirth, C., Brandt, U., Hunte, C. & Zickermann, V. (2016). Structure and function of mitochondrial complex I. *Biochimica et Biophysica Acta (BBA) - Bioenergetics,* 1857(7), 902-914.

Figure legends

Figure 1: Flies with neuronal *ND23* knockdown exhibit shortened lifespan, behavioral abnormalities and reduced ATP production

(A) RT-qPCR assays showing reduced levels of *ND23* transcripts in flies expressing the RNAi under the control of the neuronal *elav-GAL4* driver. Transcript levels of *ND23* (filled bar) were expressed in percent relative to controls (*elav>w*^{1118}) (grey bar) and represent the means ± SEM of at least 6 RNA experiments prepared from heads at the first day of adult age. The unpaired t-test shows a significant difference in mRNA levels between the RNAi-induced and control genotypes (**, p= 0.0011). (B) Lifespan of flies expressing the *ND23* RNAi in neurons was significantly reduced by comparison with control flies (*elav> w*^{1118}) as tested by the log-rank test (***, p<0.001). In this representative experiment, the mean lifespan was 85 days for control flies (open circles), 29 days for knockdown flies (filled circles) with n=58 and 50 flies, respectively. (C) Locomotor performance evaluated by negative geotaxis test on 1 day- and 4 day-old flies expressing the *ND23* RNAi transgene under the control of *elav-GAL4* by comparison with control flies (*elav>w*^{1118}). For each column, the percentages of flies climbing to the top (dark grey), remaining at the bottom (black) or staying along the geotaxis column (light grey) are depicted. Results correspond to the means ± SEM of a representative experiment (1 day: n=56 and 56 flies; 4 days: n=24 and 31 flies, respectively for each genotype). Comparisons were performed by unpaired Student's t-test (at 1 day, for the top and for the bottom: p<0.0001; at 4 days, for the top: p<0.0001 and for the bottom: p=0.0023). (D) ATP level means per brain in neuronal *ND23* knockdown of 1 day-old flies (black bar) were expressed relative to control values (*elav>w*^{1118}) (grey bar) from 3 independent experiments. Error bars represent SEM; *, p= 0.014 for unpaired t-test.

Figure 2: Neuronal knockdown of *ND23* causes neurodegeneration in the retina

(A) Representative pictures of ommatidia of control *elav>w*^{1118} and *elav>ND23* RNAi flies at 1 day, 4 days and 12 days. At 12 days, the rhabdomeres were diffuse and cannot be truly counted. (B) Photoreceptor frequency diagram at 1 day and 4 days post-eclosion with *ND23* RNAi (black bars), and control (*w*^{1118}) (grey bars) under the control of *elav-GAL4*. Statistical significances on photoreceptor frequency distributions were determined by Mann-Whitney test (at day 1, p>0.05; at day 4, p=0.0139). (C) Histology of *ND23* RNAi-expressing retina using toluidine blue staining shows small rare vacuoles (arrow) at 4 days of adult life. At 20 days, the retina developed larger vacuoles (arrows). Scale bar: 25 µm.

Figure 3: Neuronal *ND23* knockdown leads to selective axonal alteration in mushroom bodies without affecting central brain histology

(A-D) Brain histology of control (*elav*>w^{1118}) (A, C) and neuronal *ND23* knockdown (*elav*>ND23 RNAi) (B, D) flies at 4 days and 20 days. Representative images of toluidine blue-stained frontal sections taken at different brain depth levels showing the cortical and neuropile regions reveal no obvious abnormalities in the different genotypes. Higher magnification images (lower panel) show the neuronal cell bodies and cortex glia cells concentrated in cortical regions whereas the neuropile is located in the central region, both presenting no abnormalities. Scale bar: 100 µm (upper panel), 10 µm (lower panel). (E, F) Representative confocal stacks of mushroom bodies lobes of 12-day old flies visualized using Fas II immunostaining in control (*elav*>w^{1118}) (E1, E2) and neuronal knockdown brains (F1, F2). The arrows indicate the ϒ-lobe position. Scale bar: 100 µm. (G) Quantitative analysis of FasII fluorescence intensity in the mushroom body lobes expressed in arbitrary units. The results are the mean ± SEM obtained from 6 control (*elav*>w^{1118}) and 4 knockdown animals and are significantly different as determined by unpaired t-test (**, p= 0.0024). Note that the ϒ-lobes are especially altered in *ND23* knockdown flies.

Figure 4: Overexpression of the glucose transporter hGluT3 improves the phenotype of the neuronal *ND23* knockdown flies

(A) The survival of flies carrying *ND23* RNAi and *hGluT3* transgenes (filled circles) driven by *elav-GAL4* was strongly ameliorated compared with flies carrying *ND23* RNAi (grey circles) (log-rank test: **, p=0.01). Survival of control flies (*elav*>w^{1118}, open circles) was significantly higher than the survival of flies with *ND23* RNAi and *hGluT3* transgenes (log-rank test: *, p=0.0378). In this representative experiment, the lifespan of control flies was 83 days (n=81), the lifespan of *ND23* knockdown flies was 33 days (n=87), and the lifespan of flies with *ND23* RNAi and *hGluT3* was 71 days (n=78). (B) The climbing capacity of 12 day-old *ND23* knockdown flies was totally rescued in the presence of *hGluT3*. The geotaxis analysis indicates significant differences between *ND23* RNAi (n=54) and *ND23* RNAi with *hGluT3* (n=63) as determined using ANOVA and Dunnett's multiple comparison test (top: ***, p= 0.0009; bottom: ***, p<0.0001). (C) Pseudopupil analysis at 4 days shows that *hGluT3* increases the number of ommatidia with 7 rhabdomeres; the distribution of the rhabdomeres between the three genotypes was significantly different as tested by non-parametric ANOVA (p=0.0426). At 20 days, 83% of ommatidia in flies carrying *ND23* RNAi and *hGuT3* transgenes still possess 4, 5 or 6 photoreceptors. Most of photoreceptors have disappeared in animals with *ND23* RNAi and were not counted. Mann-Whitney test indicates a significant difference between the control (*elav*>w^{1118}) and *ND23* RNAi with *hGluT3* ommatidia (p=0.0281). (D) ATP levels measured in dissected 12 days-old adult brains were not statistically different between the following genotypes: *elav*>w^{1118} (control: open bar), *elav>hGluT3* (grey bar) and *elav>ND23* RNAi; *hGluT3* (black bar) as analyzed using ANOVA. Error bars represent SEM.

Figure 5: Overexpression of the glycolytic enzyme PFK does not rescue the phenotype of neuronal *ND23* knockdown

(A) Transcript levels of *PFK* of 5-day post-eclosion female heads were analyzed by RT-qPCR. The means were expressed as time-fold relative to *elav>w*^{1118} (control). Error bars represent SEM. ANOVA test and Bonferroni's multiple comparison test indicate that the levels of PFK transcripts were significantly increased in *elav>PFK* (***, p=0.0001) and *elav>ND23* RNAi; *PFK* (*, p=0.0344) by comparison with *elav>w*^{1118} and *elav>ND23* RNAi, respectively. (B) Overexpression of *PFK* (*elav>ND23* RNAi; *PFK*) (open circles) did not significantly change the survival of flies with neuronal *ND23* RNAi (filled circles) as indicated by the log-rank test. In this representative experiment, the lifespan of *elav>ND23* RNAi flies was 30 days (n=54) and the lifespan of flies with *ND23* RNAi and *PFK* was 34 days (n=63). (C, D) Representative pictures showing that overexpression of *PFK* (*elav>ND23* RNAi; *PFK*) at 4 days did not prevent photoreceptor loss by comparison with ommatidia of neuronal knockdown flies.

Figure 6: The glial knockdown of *ND23* induces vacuolization in the brain but does not modify lifespan and locomotion behavior

Toluidine blue stained frontal sections of brain from control flies (*repo>w*^{1118}) at 4 days (A1, A2) and 20 days (D1, D2) that do not show vacuoles nor dark puncta at 4 days and 20 days. Images of glial *ND23* knockdown brain show that the morphology of the cortex and neuropile is strongly altered at both 4 days (B1, B2) and 20 days (E1, E2) (arrows). At 4 days, degenerative vacuoles (arrows) invade the cortex where nuclei and soma of neurons and cortex glia are gathered. At 20 days, vacuoles with different intensities of staining are observed (black and white arrows). Dark puncta (arrowheads) are located at the border of cortex-neuropile in the *ND23* RNAi brain at 4 days and are also observed into the neuropile structure at 20 days (B2, E2, arrowheads). In the brain of flies carrying *ND23* RNAi and *hGluT3* transgenes (C1, C2), strong vacuolization (arrows) and dark puncta at the cortex-neuropile border (arrowhead) are observed. Scale bar in A1-E1: 75 µm, in A2-E2: 10 µm. (F) Lifespan of flies expressing the *ND23* RNAi in glial cells (filled circles) under the driver *repo-GAL4* was not different from that of control flies (*repo>w*^{1118}) (open circles) as tested by log-rank test. In this representative experiment, 121 and 51 flies were used, respectively. (G) Negative geotaxis assays indicate no significant motor dysfunction in flies expressing *ND23* RNAi under the control of the glial driver *repo-GAL4* at 12 days compared to the control flies (*repo>w*^{1118}). Open columns show the percentages of flies observed at the top of the column and filled columns represent the percentages of flies remaining at the bottom. Data are the means ± SEM of the percentages obtained from a representative experiment with 64 flies for both genotypes. Comparisons performed using unpaired Student's t-test do not indicate significant difference ($p>0.05$).

Figure 7: Glial knockdown of *ND23* induces accumulation of lipid droplets in the brain

(A1-C3) Bodipy 493/503 staining of LDs in control brain (*repo>w*^{1118}) (A1-A3), and in the brain of flies with glial expression of *ND23* RNAi (*repo>ND23* RNAi) (B1-B3) or *ND23* RNAi and *hGluT3* (C1-C3).

Representative stacks of 8 confocal images (1 µm interval) at 4 days are taken at different brain depth levels: near the anterior face showing the antennal lobes (AL) (A1, B1, C1), and more deeply as noted by the presence of the ellipsoid body (EB) (A2, B2, C2). Bodipy-positive puncta (green) are highly enriched in *repo>ND23* RNAi and in *repo>ND23* RNAi; *hGluT3* brains. At high magnification (A3, B3, C3), single confocal section shows green puncta labeled by Bodipy surrounding the neuropil in the glial *ND23* RNAi brain (B3) and when the *hGluT3* transgene is present (C3), whereas only few puncta are seen in the control (A3). (D) Quantification of the LD density (number of LDs per an area of 0.01 mm^2) indicates that the mean density of LDs in *repo>ND23* RNAi and *repo>ND23* RNAi; *hGluT3* brain are significantly higher than in control brains (*repo>*w^{1118}). ***, $p<0.0001$ using ANOVA and Dunnett's multiple comparison test. (E) Distribution of the LD size (μm^2) in the different genotypes showing that the number of large LDs (area>3 μm^2) is significantly increased in *repo>ND23* RNAi brains by comparison with controls (ANOVA with Bonferroni's post-test, $p=0.016$). (F-I) Confocal stacks showing the expression of the YFP-tagged perilipin2 (*plin-2::YFP*). Anti-GFP immunostaining shows sparse plin-2-positive LDs in the control *repo>plin-2::YFP* brain (F1, F2) and numerous LDs in the brain with glial *ND23* knockdown (*repo>ND23* RNAi*, plin-2::YFP*) (G1, G2) at 4 days. At high magnification (F2, G2), plin-2 is visualized as GFP fluorescent rings surrounding LDs. (H, I) Confocal stacks showing that YFP-tagged perilipin2 is not detected in *elav>plin-2::YFP* (H) and *elav>ND23* RNAi; *plin-2::YFP* (I) brain. Scale bars: 50 µm in A1-C2, F1, G1, H, I; 20 µm in A3-C3; 10 µm in F2, G2.

Figure 8: Brain ultrastructural alterations are induced by glial *ND23* knockdown

(A, C) The ultrastructure of control brain with neuronal (*elav>*w^{1118}) or glial (*repo>*w^{1118}) drivers presents neuronal cell bodies (N) enwrapped by thin extensions of glial cells (arrows) and held tight in the cortex. The cortex and neuropile are divided by a neuropile glial cell (g). In neuropile, neuronal and glial processes are intermingled, numerous mitochondria (m) are visible. Axon bundles (ax) are recognizable. (B, D) The brain of neuronal knockdown flies presents no obvious ultrastructural alteration (B, *elav>*ND23 RNAi). In contrast, glial knockdown brain (D1-D3*, repo>ND23* RNAi) shows several abnormalities. Vacuoles (v) are predominantly scattered among neuronal cell bodies (N) and present various sizes and contents of unorganized material (D1, D3). Numerous LDs are observed as electron-dense, homogeneously filled particles at the cortex-neuropile junction (D2, D3). They can be in tight contact with mitochondria (m) (D2 and inset). Scale bar: 2 µm in A-D2; 1 µm in D2 inset; 5 µm in D3.

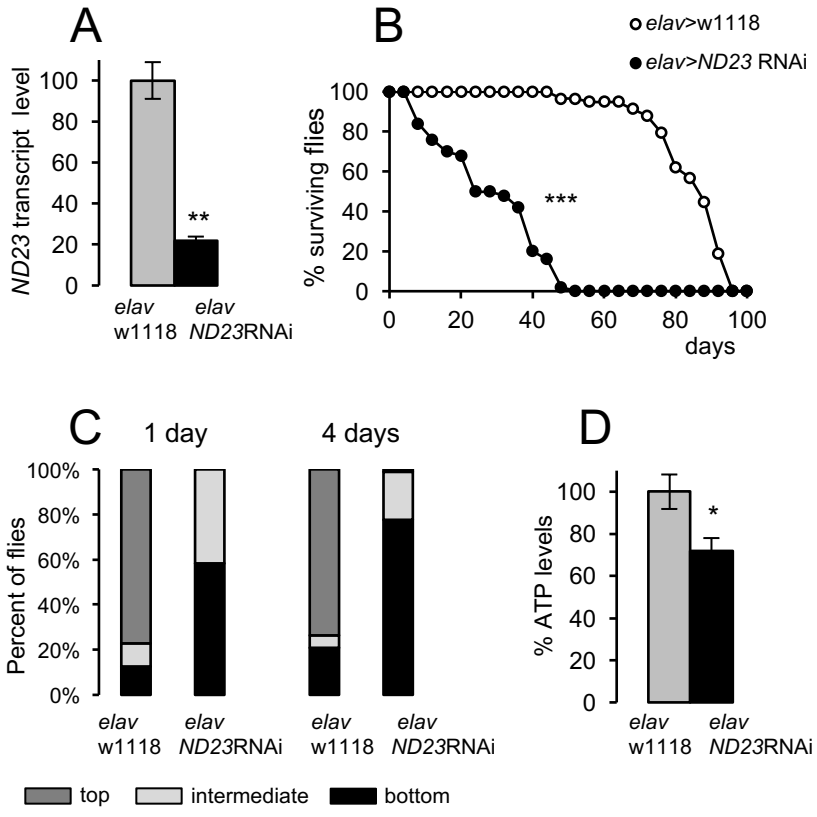

Fig. 1 CABIROL

11.85x11.23

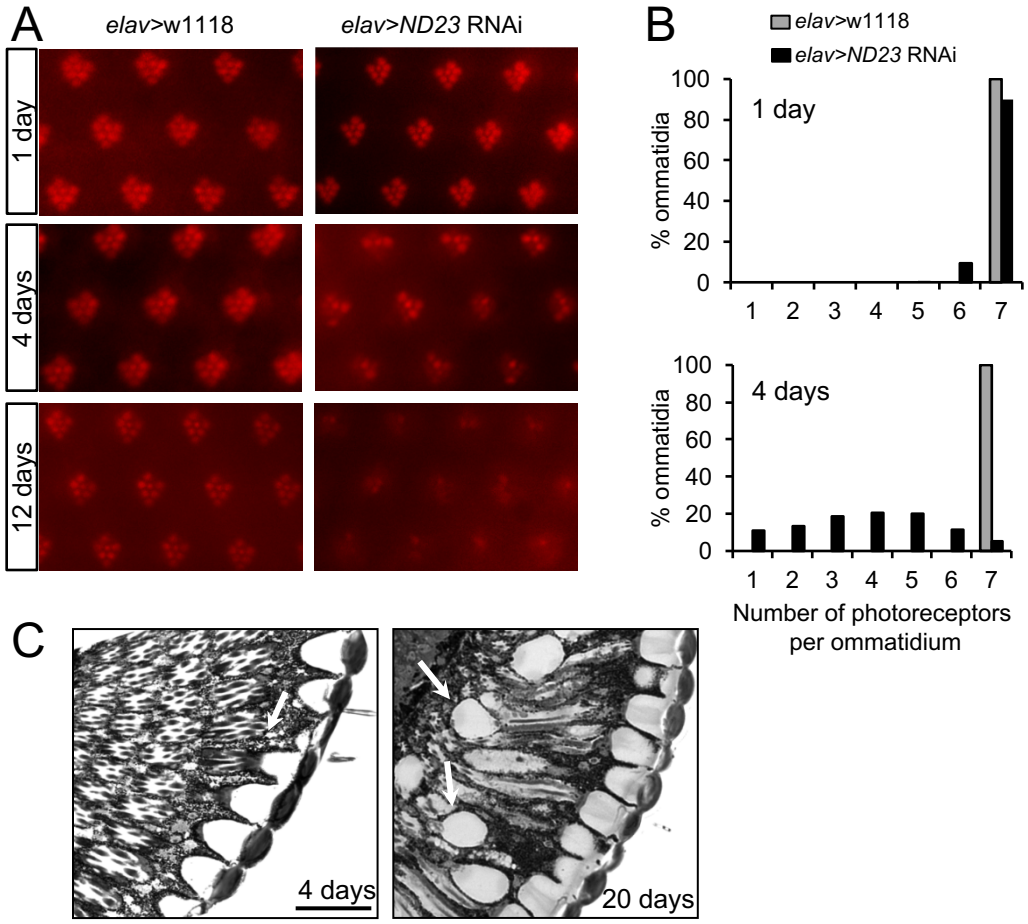

Fig. 2 CABIROL

13.31x15

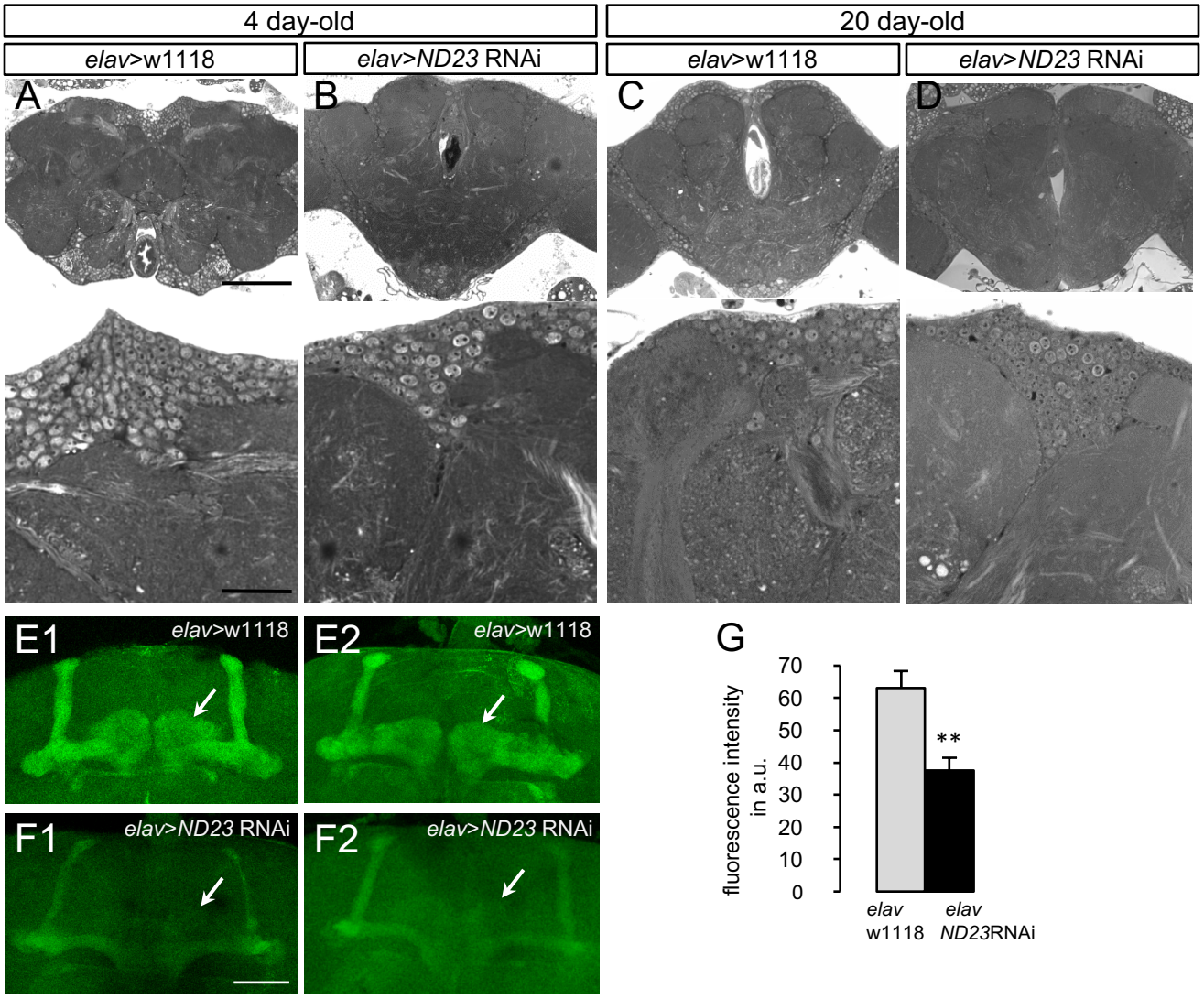

Fig. 3 CABIROL

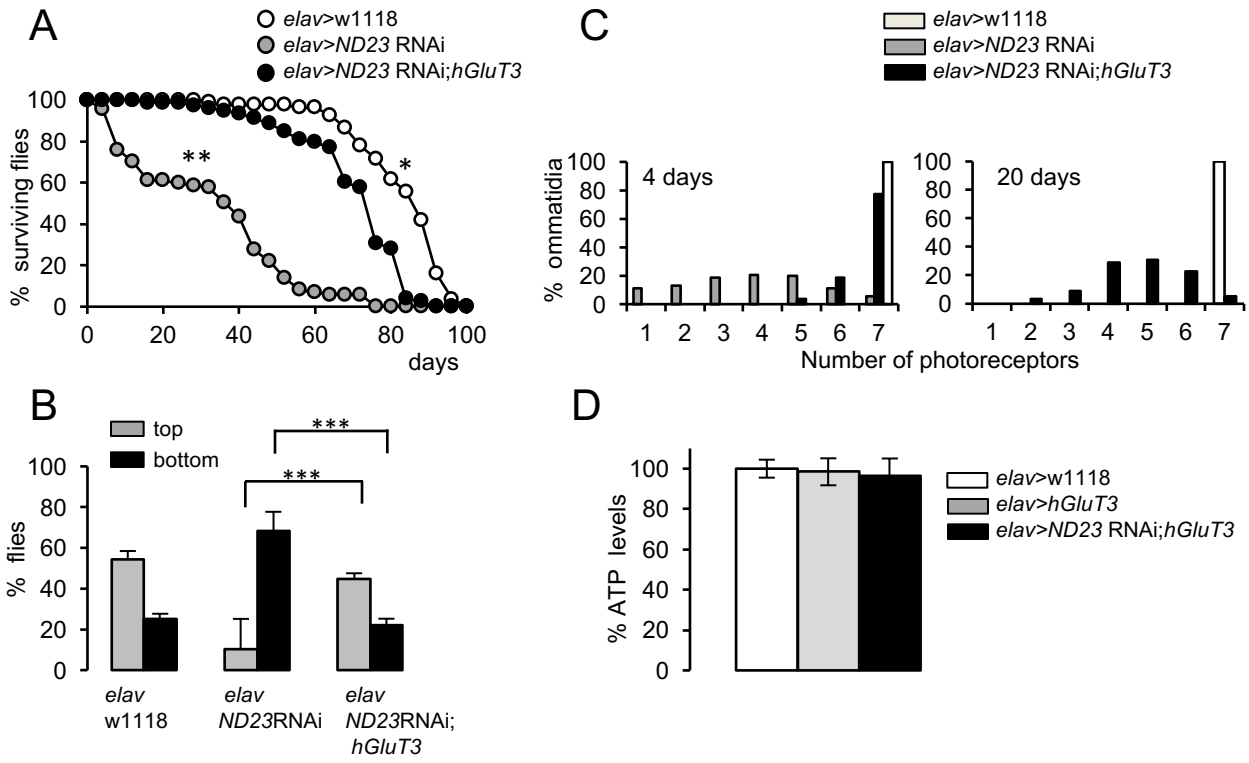

Fig. 4 CABIROL

10.43x17.03

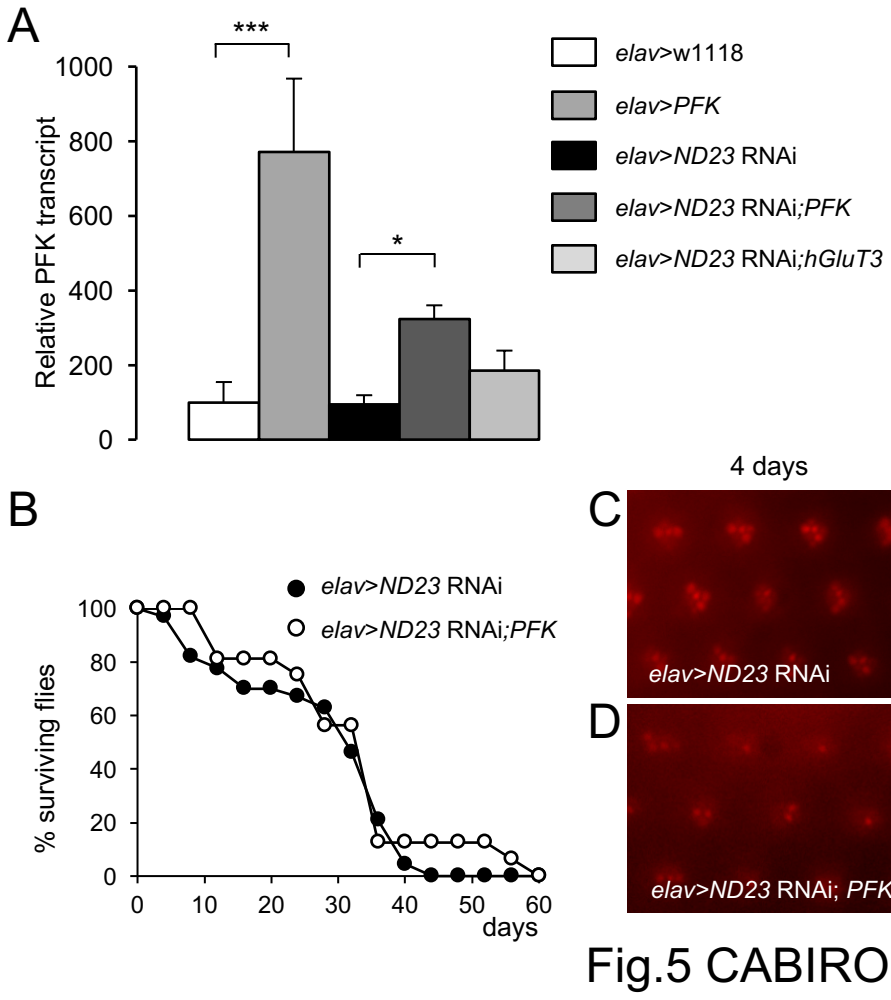

Fig.5 CABIROL

13.47x12.58

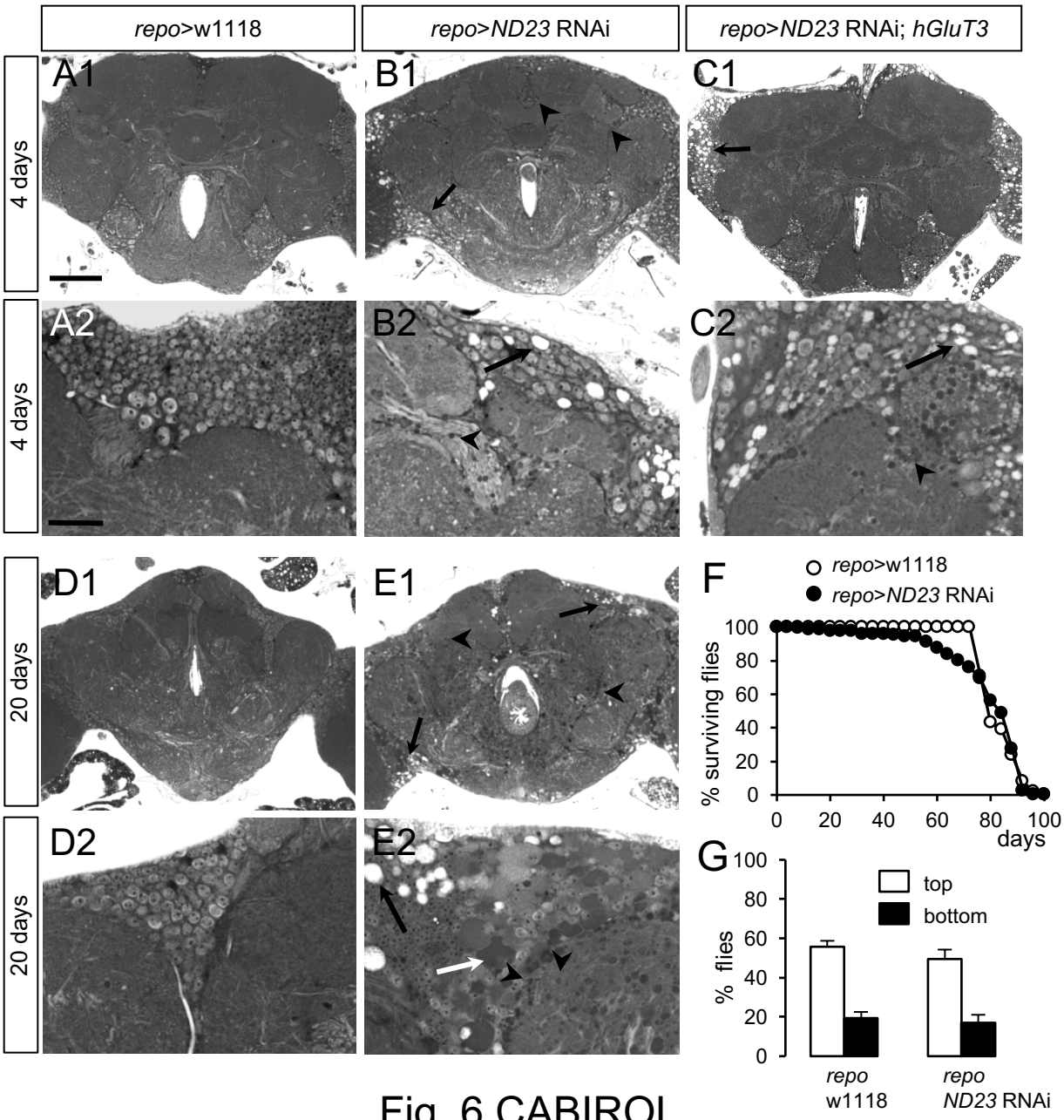

Fig. 6 CABIROL

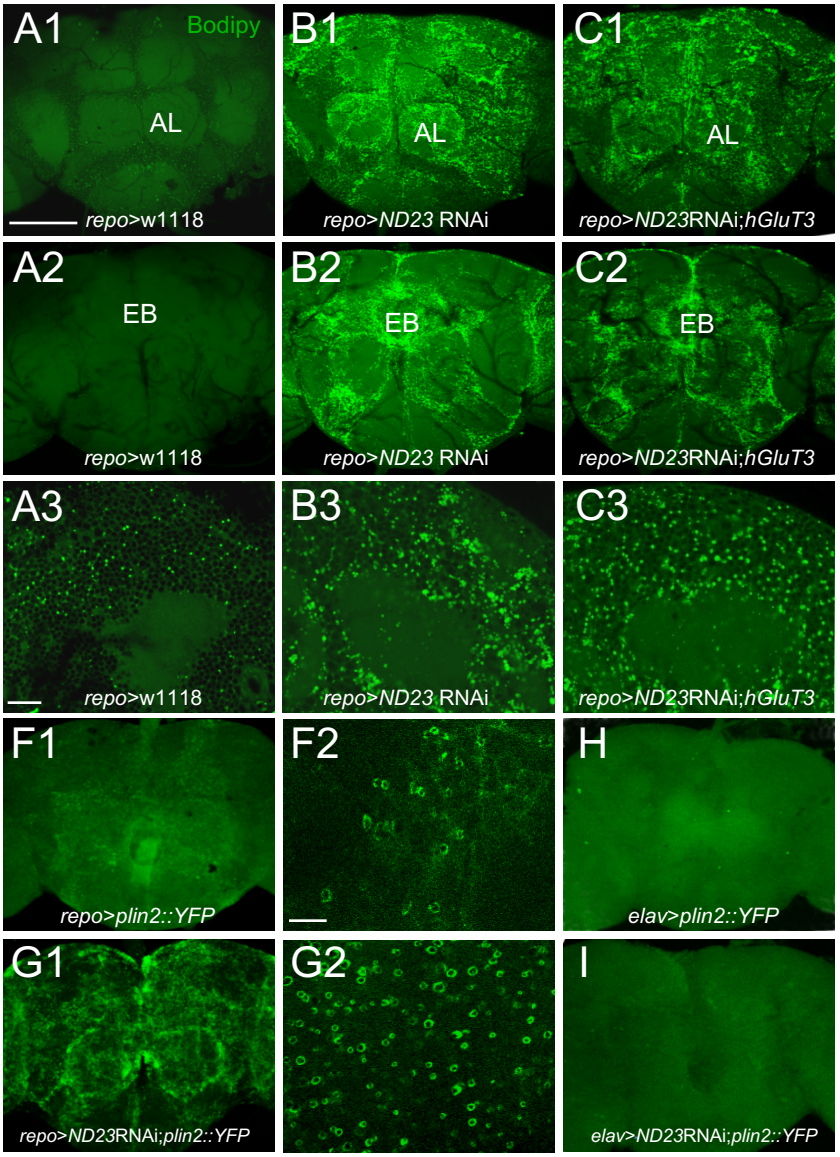

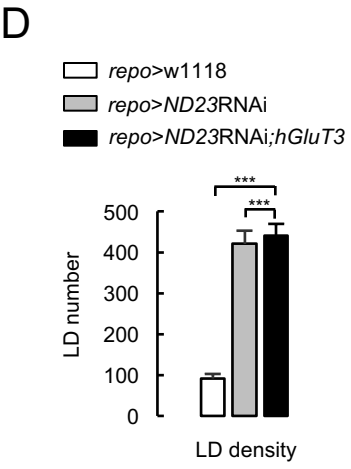

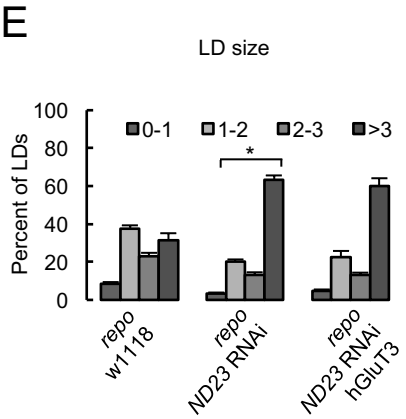

Fig. 7 CABIROL

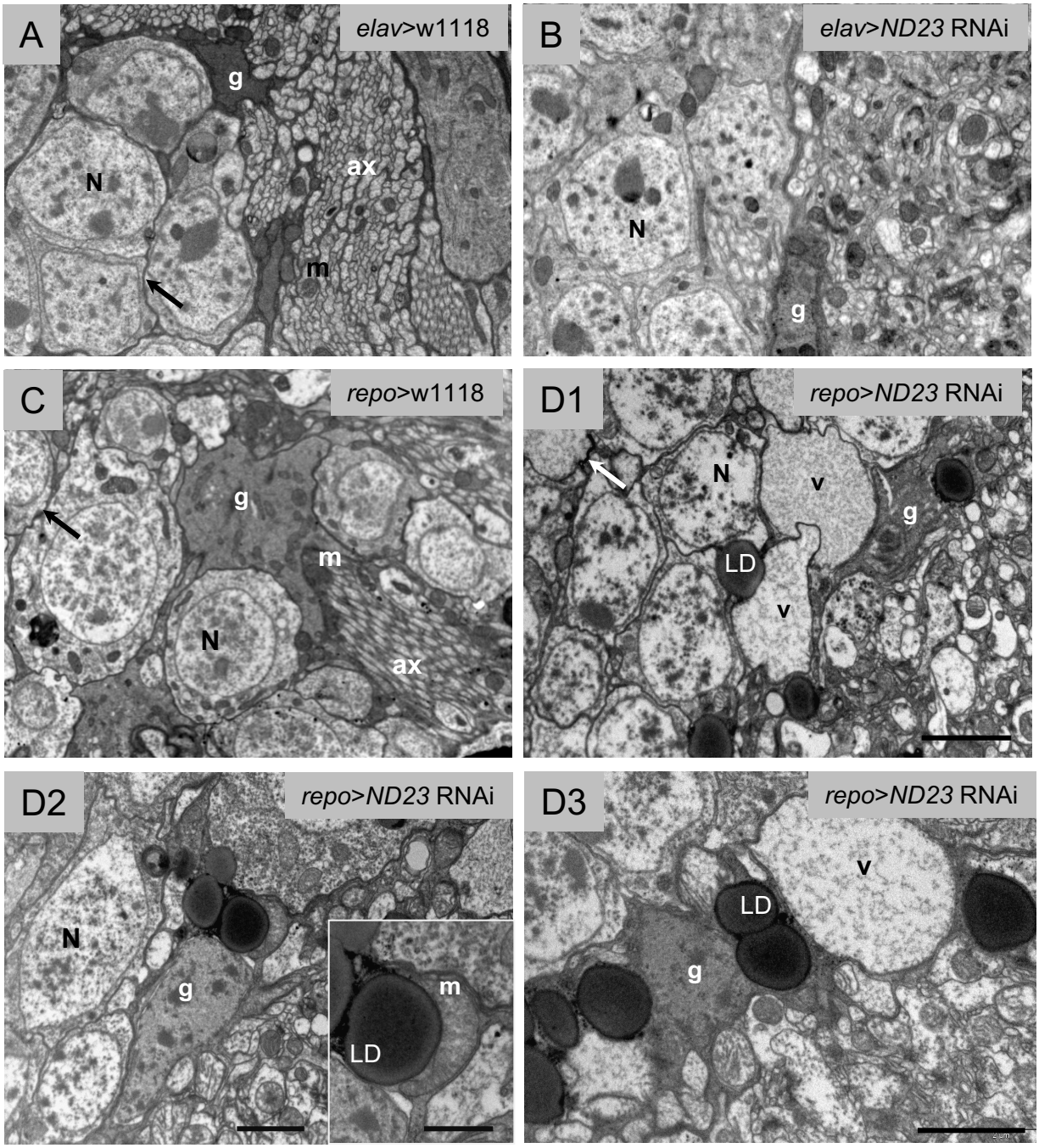

Fig. 8 CABIROL

12.92x16.21